



OPEN ACCESS

EDITED BY
Katarina Polcicova,
Slovak Academy of Sciences, Slovakia

*CORRESPONDENCE
Zhaoxiang Wang,
624429498@qq.com
Keyu Zhang,
z_cole@sina.com

[†]These authors have contributed equally
to this work

RECEIVED 17 October 2022
ACCEPTED 18 April 2023
PUBLISHED 23 June 2023

CITATION
Huang Z, Zheng H, Wang Y, Wang X,
Wang C, Liu Y, Zhou W, Wang Z and
Zhang K (2023), The modulation of
metabolomics and antioxidant stress is
involved in the effect of nitazoxanide
against influenza A virus *in vitro*.
Acta Virol. 67:11612.
doi: 10.3389/av.2023.11612

COPYRIGHT
© 2023 Huang, Zheng, Wang, Wang,
Wang, Liu, Zhou, Wang and Zhang. This
is an open-access article distributed
under the terms of the [Creative Commons Attribution License \(CC BY\)](https://creativecommons.org/licenses/by/4.0/).
The use, distribution or reproduction in
other forums is permitted, provided the
original author(s) and the copyright
owner(s) are credited and that the
original publication in this journal is
cited, in accordance with accepted
academic practice. No use, distribution
or reproduction is permitted which does
not comply with these terms.

The modulation of metabolomics and antioxidant stress is involved in the effect of nitazoxanide against influenza A virus *in vitro*

Zhen Huang^{1,2†}, Haihong Zheng^{1†}, Yanping Wang¹,
Xiaoyang Wang¹, Chunmei Wang¹, Yingchun Liu¹, Wen Zhou¹,
Zhaoxiang Wang^{2*} and Keyu Zhang^{1*}

¹Key Laboratory of Veterinary Chemical Drugs and Pharmaceuticals, Ministry of Agriculture and Rural Affairs, Shanghai Veterinary Research Institute, Chinese Academy of Agricultural Sciences, Shanghai, China, ²College of Animal Science, Yangtze University, Jingzhou, Hubei, China

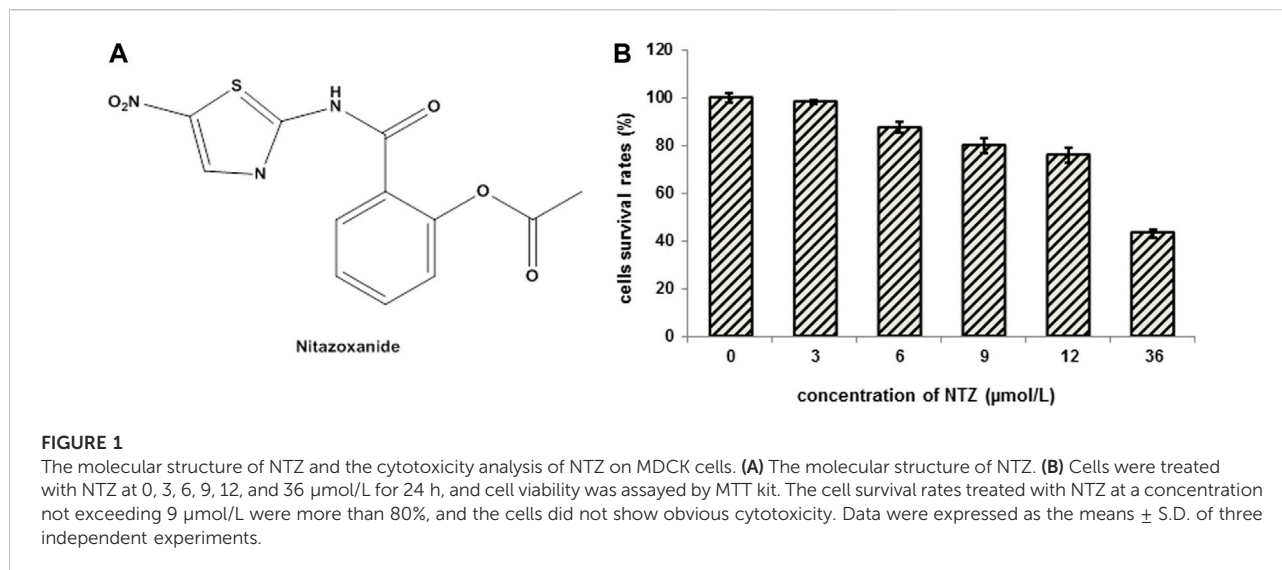
The prevalence of highly infectious influenza A virus (IAV) is still a major threat to global human health. Nitazoxanide (NTZ) possesses potent antiviral properties against the influenza virus. However, the role of small molecular metabolites and antioxidant stress in the NTZ's anti-influenza virus mechanism is not yet fully understood. This study compared the changes in cellular metabolism, ROS levels, antioxidant enzyme activities, and Keap-1/Nrf2 pathway in IAV-infected MDCK cells after NTZ treatment *in vitro*, using LC-MS-based metabolomics, flow cytometry, immunoblot. We observed that the NTZ treatment in the IAV-infected cells drastically altered the metabolism of small molecules, among which eleven metabolites were highly relevant to NTZ. The virus induced oxidative stress was also remarkably suppressed by NTZ. Meanwhile, the Nrf2 pathway and some proteins with modulating antiviral activity were activated after NTZ treatment, protecting cells from IAV injury. Therefore, regulation of the intracellular oxidative state is the primary outcome of NTZ treatment, which may underpin an antiviral mechanism attributed to the thiazolide.

KEYWORDS

nitazoxanide, influenza A virus, metabolomics, anti-oxidative stress, Nrf2

Introduction

Influenza A virus (IAV) typically infects epithelial cells of the upper and lower respiratory tracts, causing oxidative stress and inflammation that can contribute to highly contagious acute respiratory illness and even death (Lindstrom et al., 2012; Tian et al., 2019). The approved antiviral drugs, including oseltamivir, amantadine and baloxavir marboxil, play important roles in combating IAVs. However, the emergence of viruses with drug resistance is rendering current drugs ineffective (Zhao et al., 2020). Devastating epidemic or pandemic events may be caused by novel IAVs with increased fitness, pathogenicity and drug resistance. Thus, discovering next-generation anti-influenza drugs is crucial in addressing this issue.



Nitazoxanide (NTZ, Figure 1A) or 2-(acetyloxy)-N-(5-nitro-2-thiazolyl) benzamide was first developed as a cestocidal agent for veterinary by Rossignol in the early 1970s (Rossignol, 2014). In Latin America, Egypt, Bangladesh and India, NTZ has also been widely commercialized as an oral broad spectrum antiparasitic agent with high safety for the treatment of intestinal parasitic infections (Rossignol, 2014; Stachulski et al., 2021). In addition to antiparasitic infection, the broad spectrum antibacterial activity, antiviral activity as well as anti-inflammatory effect of NTZ have been highlighted in recent years (Dubreuil et al., 1996; Odingo et al., 2017; Shou et al., 2019; Stachulski et al., 2021). A series of *in vitro* studies have also demonstrated that NTZ could effectively inhibit the replication of various influenza A strains including oseltamivir- and amantadine-resistant strains with different mechanisms (Rossignol et al., 2009). The current threat from pandemic virus has promoted further research into the potential of NTZ as an antiviral agent for the treatment for both influenza and COVID-19.

Metabolomics uses analytical chemistry approaches to broadly profile the endogenous small molecule metabolites involved in diverse cellular processes, including mitochondrial function, lipid biosynthesis and metabolism, and nucleotide biosynthesis, and therefore is most closely correlating with biological phenotype. Comparative metabolic profiling under drug-treated and untreated conditions provides a powerful strategy for understanding the mechanisms of drug action at the molecular level (Wiklund et al., 2008). There is still a great speculation surrounding the mechanisms of action of NTZ, like the effect of NTZ on the influenza virus-induced endogenous molecule metabolites and oxidative stress is unknown. By a metabolic profiling approach, our study investigated NTZ's anti-influenza effect by focusing on a number of metabolites from Madin-Darby canine kidney (MDCK) cells with different treatment. The effects of NTZ on Nrf2 that adjusts cell responses against influenza virus-induced oxidative and electrophilic stress is also discussed.

Materials and methods

Chemical and biological materials

Nitazoxanide (NTZ, purity \geq 98.5%, Figure 1A), influenza A virus (IAV) A/Puerto Rico/8/34 (H1N1) (PR8) and Anti-NP (influenza virus nucleoprotein) mAbs were obtained from Shanghai veterinary research institute, Chinese academy of agricultural sciences. NTZ was dissolved with DMSO and stored at -20°C . Fetal bovine serum (FBS) and Dulbecco's modified Eagle's medium (DMEM) were purchased from Gibco (Auckland, NZ). Anti- β -actin (CST, 3700), anti-Lamin B1 (CST, 13435), anti-Keap1 (CST, 8047), anti-Nrf2 (CST, 12721), anti-NQO1 (CST, 3187), anti-GSTP1 (CST, 3369), anti-PKR (CST, 12297), anti-Phospho-eIF2 α (CST, 3398), anti-LC II (CST, 4108S) antibodies were purchased from Cell Signaling Technology (Beverly, MA, United States). HRP-conjugated anti-rabbit and anti-mouse secondary antibodies were purchased from Abcam Inc. (Cambridge, MA, United States). MTT assay kit, PVDF membrane, reactive oxidant species (ROS) assay kit, catalase (CAT) assay kit, total superoxide dismutase (SOD) assay kit with WST-8, RIPA buffer and nuclear-cytosol extraction kit were also purchased from Beyotime Biotechnology (Shanghai, China).

Cell and virus culture

Madin-Darby canine kidney (MDCK) cells were maintained in DMEM containing 10% FBS at 37°C in a moist atmosphere with 5% CO_2 and 95% air. When the cells confluence completely, they were infected with PR8 virus in the presence or absence of NTZ. The viability of MDCK cells was evaluated using MTT assay kit according to the manufacturer's instructions (Beyotime Biotech Inc., China).

Anti-influenza activity of NTZ

Confluent MDCK cell monolayers were infected with IAV (PR8) at 37°C at 100 TCID₅₀. The viral inoculum was removed after 1 h of coculture, and cell monolayers were washed three times with phosphate-buffered saline (PBS). The cells were incubated at 37°C in DMEM culture medium with different concentration (0, 3, 6 or 9 µmol/L) of NTZ. Virus yield was determined 24 h post-infection (p.i.) by Hemagglutination assay (Bernasconi et al., 2005). Further, the expression of IAV nucleoprotein was detected by Western blot analysis with anti-NP mAbs.

The treated cells for metabolomic profiles

The MDCK cells for metabolomic profiling study were divided into four groups: group C was the cells without any treatment; group C+N was the cells treated with NTZ; group V was the cells infected by IAV PR8 influenza virus; and group V+N was the cells infected with IAV PR8 virus and treated with NTZ. The IAV PR8 at 3 TCID₅₀ was used for infection groups (group V and group V+N), and the dose for NTZ treatment (group C+N and group V+N) was 3 µmol/L. The cells were then incubated in DMEM for 24 h at 37°C in 5% CO₂ incubator.

Metabolites extraction

Metabolites extraction was performed as reported previously (Ritter et al., 2010; Tian et al., 2019). Briefly, all solutions used were ice-cold. The treated cells were washed twice with PBS followed by an immediate addition of 60% methanol containing 0.85% ammonium bicarbonate by vortex for 10 s at 4°C. Then the lysates were centrifuged at 1,000 rpm for 1 min at 4°C, the supernatants were discarded and 1.0 mL extract solution (acetonitrile: methanol: water = 2: 2: 1, v/v) containing isotopically-labelled internal standard (2-Chloro-L-Phenylalanine) mixture was added to the samples, which were then vortexed for 30 s. After three cycles of homogenization at 35 Hz for 4 min and sonicated for 5 min in an ice-water bath, the samples were incubated at -40°C for 1 h and centrifuged at 12,000 rpm for 15 min at 4°C. The resulting supernatant was transferred to a fresh glass vial for HPLC-MS analysis.

LC-MS/MS analysis

As described previously (Ritter et al., 2010; Tian et al., 2019), the metabolomics analysis was performed using a 1290 infinity series UHPLC System (Agilent Technologies) coupled to a QE mass spectrometer (Q Exactive Focus, Thermo) equipped with an

electrospray ionization (ESI) source. The chromatographic separation of all samples was performed on a UPLC BEH Amide column (2.1 × 100 mm, 1.7 µm, Waters) with mobile phase A (water (pH = 9.75) consisting of 25 mmol/L ammonium acetate and 25 mmol/L ammonia hydroxide) and mobile phase B (acetonitrile). The flow rate was 0.5 mL/min with a gradient elution.

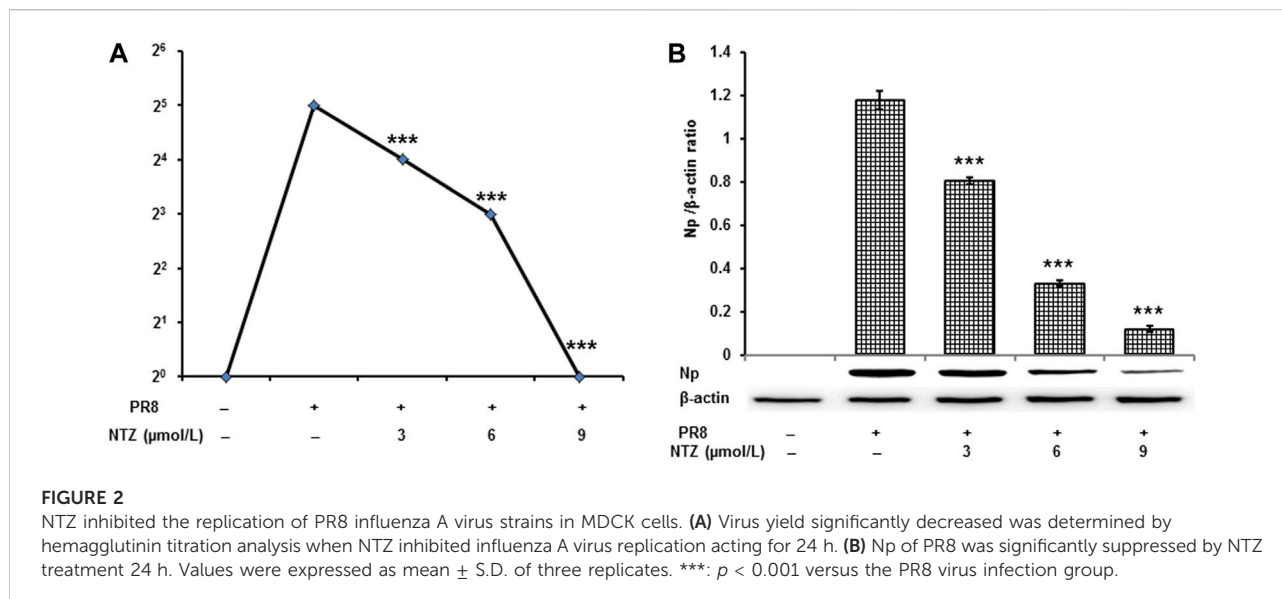
The mass spectrometer was operated in both positive-ion and negative-ion modes with the following parameters: sheath gas flow rate as 45 Arb, Aux gas flow rate as 15 Arb, capillary temperature 400°C, full MS resolution as 70,000, MS/MS resolution as 17,500, collision energy as 10/30/60 in NCE mode, spray Voltage as 4.0 kV (positive) or -3.6 kV (negative), respectively. To evaluate the stability and reproducibility of the LC-MS analytical platform during data acquisition, QC samples were analyzed.

LC-MS data processing and statistics

ProteoWizard software was used to convert the raw mass spectrometry data to the mzXML format. Peak detection, extraction, alignment, and integration were processed with an in-house program (BiotreeDB), which was developed using R and based on XCMS. Then an in-house MS² database was applied in metabolite annotation. The cutoff for annotation was set at 0.3.

In this study, the final dataset containing the information of peak number, sample name and normalized peak area was imported to SIMCA15.0.2 software package (Sartorius Stedim Data Analytics AB, Umea, Sweden) for multivariate analysis (Wiklund et al., 2008). To visualize the distribution and the grouping of the samples, PCA (principle component analysis, PCA) was applied to reduce the dimension of the data, and to identify potential outliers in the dataset with 95% confidence interval as the threshold.

Supervised OPLS-DA (orthogonal projections to latent structures-discriminate analysis, OPLS-DA) was carried out to visualize group separation and find significantly changed metabolites. The values of R^2 and Q^2 parameters were used to verify the fitness and predictive ability of the model. After a 7-fold cross validation calculated, the values of R^2 and Q^2 were obtained. The R^2 and Q^2 intercept values based on a 200 times permutation was used to further assess the robustness and predictive ability of the OPLS-DA model. Furthermore, the value of variable importance in the projection (VIP) of the first principal component in OPLS-DA analysis was performed to discriminate the contribution of each variable to the model. Differentially expressed metabolites were identified by $VIP > 1$ and $p < 0.05$ (Student's t-test). In addition, commercial databases including KEGG (<http://www.genome.jp/kegg/>) and MetaboAnalyst (<http://www.metaboanalyst.ca/>) were used for pathway enrichment analysis.



Measurement of intracellular ROS levels and antioxidant enzymes activities

Intracellular ROS and antioxidant enzymes activities were measured as previously described (Zhang et al., 2014). Briefly, the cells treated with NTZ were washed three times with PBS (pH = 7.2), and incubated with 10 μ mol/L DCFH-DA at 37°C for 20 min according to the manufacturer's instructions. DCF fluorescence was detected by CytoFLEX flow cytometer (Becton Dickinson) and fluorescence microscope. For antioxidant enzymes activities measurement, the cells were lysed with ice-cold RIPA buffer on ice for 15 min, then the cell lysates were harvested and supernatants were collected via centrifuged at 12,000 \times g for 10 min at 4°C. Protein concentrations were determined using BCA protein assay (Beyotime Biotech Inc., China) before antioxidant enzymes activities measurement. The CAT activity and the total SOD activity were quantitatively detected with OD at 520 and 450 nm, respectively.

SDS-PAGE and immunoblotting

The cells were washed twice with pH 7.4 ice-cold PBS and lysed with ice-cold RIPA buffer containing 1% phenylmethanesulfonyl fluoride (PMSF) for 15 min. The lysates were collected for concentration determination using BCA protein assay kit (Beyotime Biotech Inc., China). Thirty micrograms of protein samples were denatured by adding 5 \times SDS loading buffer followed by heating at 100°C for 10 min. Protein separation was conducted by electrophoresis on an 8%–12% SDS-Tris-glycine polyacrylamide gel. After protein transfer,

the PVDF membrane was blocked in 5% bovine serum albumin (BSA) for 2 h (blocking solution) before being incubated at 4°C overnight with the following antibodies at a dilution of 1:1,000: anti- β -actin, anti- Lamin B1, anti- Keap1, anti- Nrf2, anti-NQO1, anti- PKR, anti- Phospho-eIF2 α , anti- NP, and anti-LC II antibodies. The membranes were then washed three times with Tris buffered saline Tween-20 (TBST) for 15 min each time before the incubation with 1:5,000 goat anti-mouse IgG H&L (HRP) or goat anti-rabbit IgG H&L (HRP) at room temperature for 1 h. Finally, the membrane was visualized by Odyssey Imager (Gene Company Limited).

Statistical analysis

All assays were performed three times and their results were expressed as mean \pm standard deviation (SD). The criterion which based on the probability of $p < 0.05$ and $p < 0.01$ was used to identify significant differences between the control and exposure groups in one-way analysis of variance (ANOVA) with LSD (Least Significant Difference). All statistical analyses were performed using SPSS 22.0 (SPSS, Chicago, IL, United States).

Results

NTZ showed the activity of inhibiting IAV replication *in vitro*

MTT assay was performed to exclude the possibility that the NTZ's anti-influenza effects were due to its cytotoxicity. As

shown in [Figure 1B](#), when NTZ not exceeding 9 $\mu\text{mol/L}$ in a 24-h treatment, no obvious cytotoxicity was observed in the MDCK cells and survival rate of the treated cells was more than 80%. Therefore, the highest NTZ dose was set to 9 $\mu\text{mol/L}$ in our further experiments.

Hemagglutinin levels reflect the activity of viral replication in cells. As shown in [Figure 2A](#), the levels of viral hemagglutinin were dramatically decreased from 2^5 to 2^0 in NTZ-treated cells, which demonstrated NTZ's dose-dependent inhibition to virus replication. Furthermore, the protein level of NP of IAV PR8, which represents the survival of influenza virus, was also found to be significantly inhibited by NTZ in a dose-dependent manner in the Western blot analysis ([Figure 2B](#)).

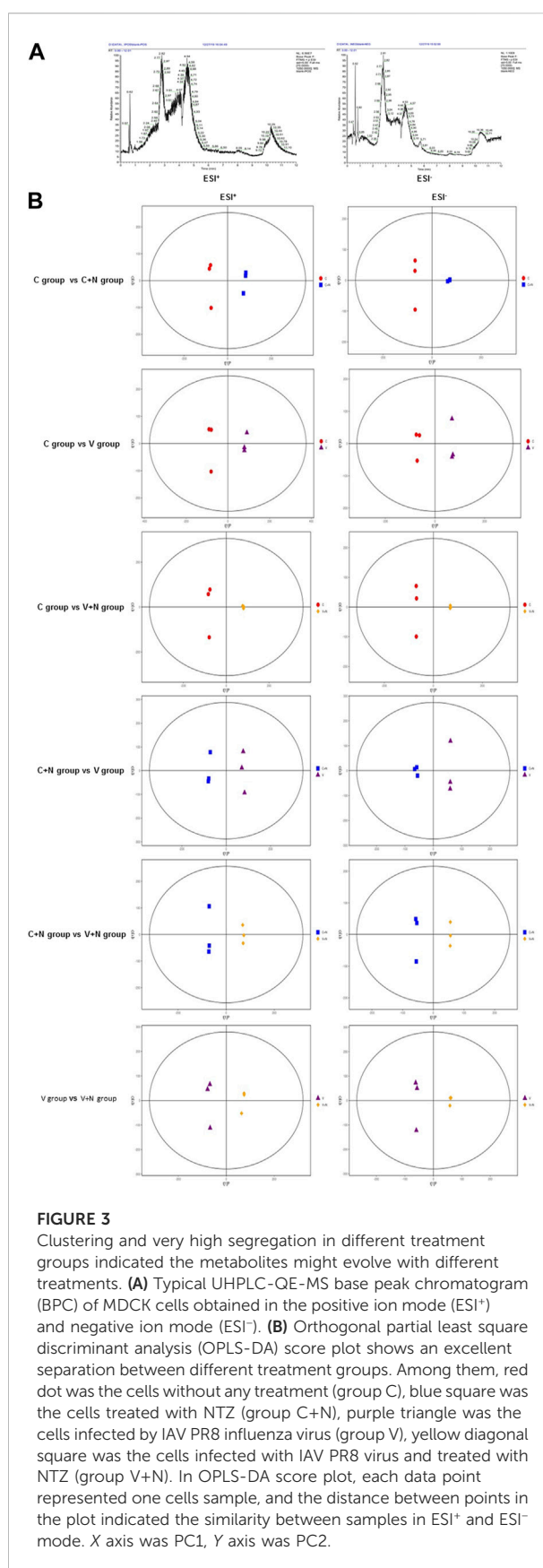
NTZ regulated the metabolic profile of cells infected IAV

Typical UHPLC-QE-MS base peak chromatogram (BPC) of cells samples from different groups (group C, group C+N, group V, and group V+N) are shown in [Figure 3A](#). Total 47,290 (20,427 in ESI⁺ and 26,863 in ESI⁻) retention time-exact mass pairs were detected. The analysis of PCA showed that the separations of samples in different groups were significant. And, as shown in [Figure 3B](#), the OPLS-DA score plots showed distinct clustering and very high segregation among groups.

In pairwise comparisons, the sum of the number of metabolites with significant difference was 466 in each group (310 in ESI⁺ and 156 in ESI⁻) ([Figure 4A](#)). In [Figures 4B, C](#) and [Supplementary Figure S1](#), we depicted the upregulated and downregulated metabolites in MDCK cells with the heat map diagrams responding to different groups, which indicate the various metabolic influences induced during different treatment.

There were many significant alterations in the levels of several metabolites between IAV infection group (group V) and cell control group (group C) ([Figure 3B](#)). The levels of adenine, 4-hydroxycitrulline, lysyl-valine, and other 32 metabolites in ESI⁺ mode ([Supplementary Figure S1](#)) in group V were found to be significantly higher than those in group C, whereas the levels of N-(2-methylpropyl) acetamide, malonylcarnitine, leucyl-glycine, and other 9 metabolites in group V were significantly lower than group C. The levels of nonanedioic acid, deoxyguanosine, 2-pyridylacetic acid, and other 27 metabolites in ESI⁻ mode ([Supplementary Figure S1](#)) in group V were found to be significantly higher than group C, whereas the levels of lipoxin A4, isonicotinic acid, 3b-hydroxy-5-cholenoic acid, and other 5 metabolites in group V were found to be significantly lower than group C.

Compare group V+N with group V, we found level alterations in a few metabolites, For example, spermidine, valyl-proline, important intermediates in amino acid metabolism and other 26 metabolites in ESI⁺ mode



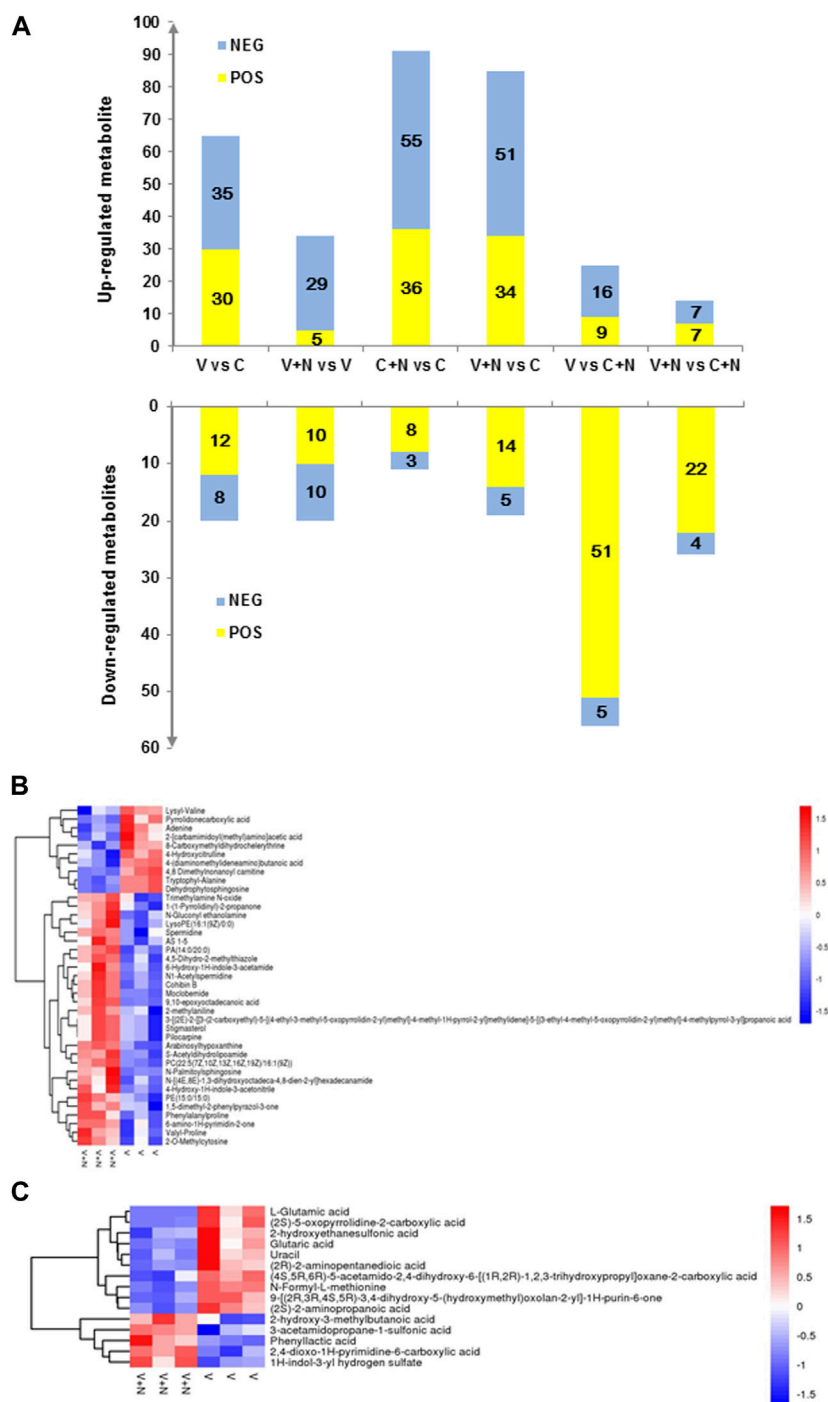
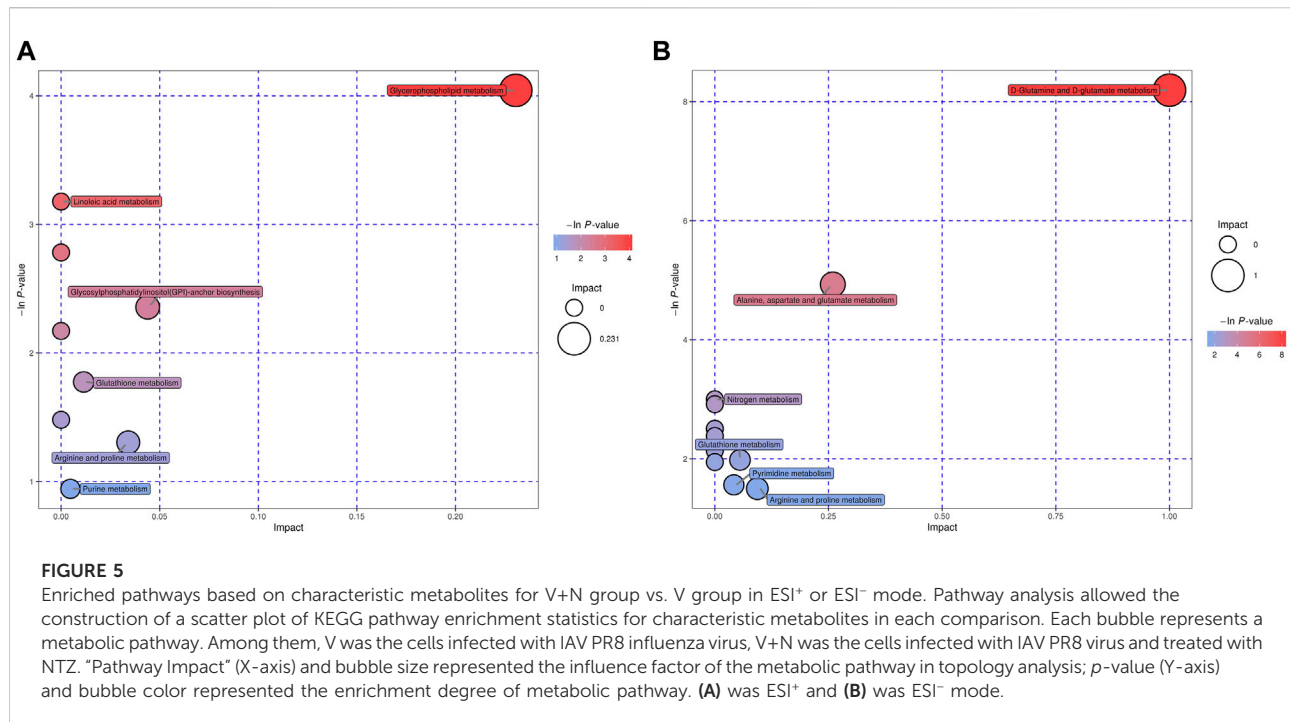


FIGURE 4

Identification and characterization of altered metabolites after different treatments. **(A)** Bar graph showing a large number of metabolite changes. The X-axis represented the different treatment groups, and the number of metabolite changed on the Y-axis. The metabolites with VIP >1 and $p < 0.05$ were significantly different. Yellow (ESI⁺ and ESI⁻) indicated upregulated, while blue (ESI⁺ ESI⁻) indicated downregulated. **(B,C)** were the heatmaps of hierarchical clustering analysis for group V vs. group V+N in ESI⁺ or ESI⁻ mode. Among them, C was the cells without any treatment (group C), C+N was the cells treated with NTZ (group C+N), V was the cells infected by IAV PR8 influenza virus (group V), V+N was the cells infected with IAV PR8 virus and treated with NTZ (group V+N). Normalized metabolite abundance (\log_2 transformed and row adjustment) were visualized as a color spectrum and the scale from least abundant to highest ranges is from -2.0 to 2.0.



(Figure 4B) were shown to be significantly more abundant in group V+N than group V. Meanwhile, the levels of some other kind of organic acids and derivatives were found to be significantly lower in group V+N than group V, including 4-hydroxycitrulline, pyrrolidonecarboxylic acid. At the same time in ESI⁻ model (Figure 4C), the levels of 1H-indol-3-yl hydrogen sulfate, phenyl lactic acid and 3-acetamidopropane-1-sulfonic acid were found to be elevated significantly in group V+N. In contrast, the level of L-glutamic acid, (2S)-5-oxopyrrolidine-2-carboxylic acid, and (2S)-2-aminopropanoic acid declined significantly in group V+N. Many of these metabolites are involved in the metabolism of important amino acids.

In addition, in group N + C, several lipids and lipid-like molecules, such as 1-hexadecyl-glycero-3-phosphate, and organic acids and derivatives, such as L-lactic acid, showed significant increases compared to the group C. Conversely, organic acids and derivatives including L-agaridoxin, hydroxyprolyl-proline and N-formyl-L-methionine significantly decreased. Obviously, these metabolites are involved in a number of complex biosynthesis and functions.

NTZ regulated the metabolic pathway of cells infected IAV

The metabolites altered were mapped into their KEGG pathways (Figure 5, Supplementary Tables S1, S2). Upon IAV infection, the most significantly activated cellular metabolite processes were D-glutamine and D-glutamate metabolism

(ESI⁺) and nitrogen metabolism (ESI⁻). However, when the IAV infected cells were treated with NTZ (group V+N), the most significantly activated cellular metabolite processes were glycerophospholipid metabolism (ESI⁺) and D-glutamine and D-glutamate metabolism (ESI⁻). The cellular metabolic changes most significantly induced by NTZ alone (group C+N) were linoleic acid metabolism (ESI⁺) and phenylalanine, tyrosine and tryptophan biosynthesis metabolism (ESI⁻).

The changes of some metabolites were closely related to the antiviral effect of NTZ

It is worth noting that 80 metabolites fluctuated with the NTZ treatment in virus-infected cells. Among them, L-glutamic acid, (2S)-5-oxopyrrolidine-2-carboxylic acid and other seven metabolites, increased significantly during viral infection (group V), but decreased significantly in both groups C and group V+N (Figure 6A). In addition, 9,10-epoxyoctadecanoic acid and 3-acetamidopropane-1-sulfonic acid significantly decreased in group V but increased in groups C and groups V + N (Figure 6A).

The list of metabolites associated with IAV infection due to drug treatment was uploaded into the enrichment analysis module of MetaboAnalyst. The results of the metabolite set enrichment analysis (MSEA) revealed a correlation between the altered metabolites and the biological function of NTZ treatment on the IAV infected cells. As showed in Figure 6B, the main functions of these metabolites were glucose-alanine cycle, alanine metabolism and glutathione metabolism in

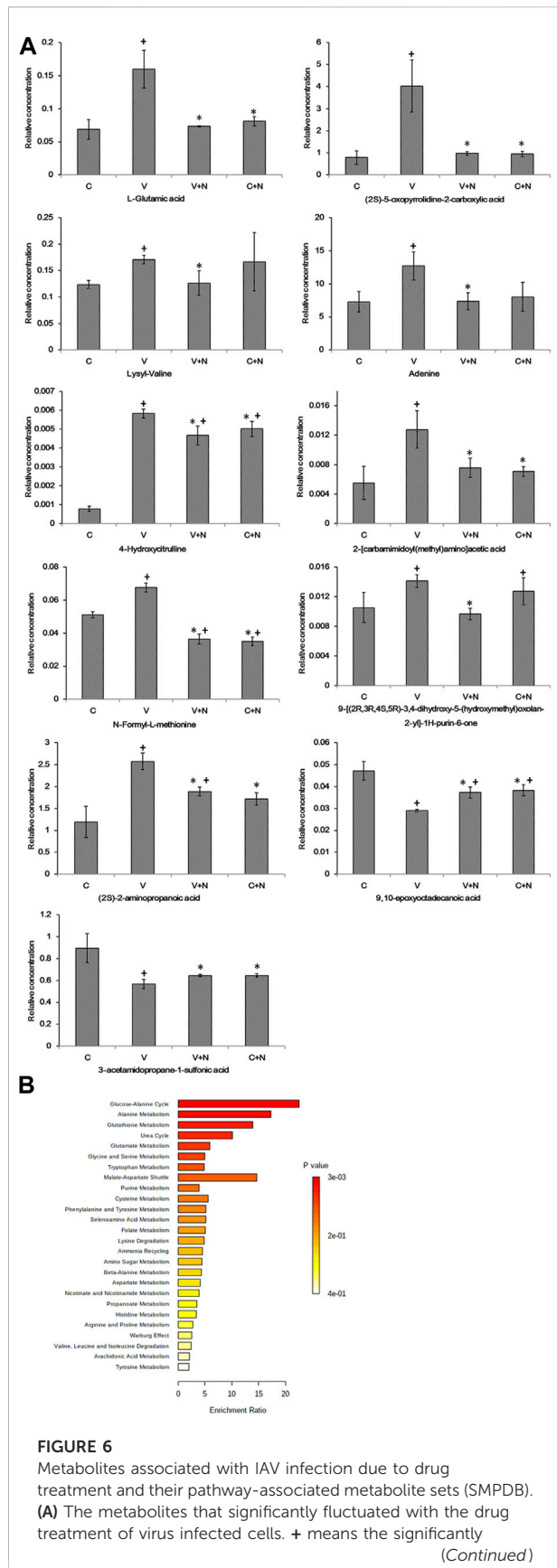


FIGURE 6 (Continued)
different ($p < 0.05$) when the group compared with control cell group; * means the significantly different ($p < 0.05$) when the group compared with IAV infection group. Among them, C was the cells without any treatment (group C), C+N was the cells treated with NTZ (group C+N), V was the cells infected with IAV PR8 influenza virus (group V), V+N was the cells infected with IAV PR8 virus and treated with NTZ (group V+N). (B) The main functions of the metabolites in pathway-associated metabolite sets (SMPDB) were revealed by the metabolite set enrichment analysis.

pathway-associated metabolite sets (Small Molecule Pathway Database, SMPDB).

NTZ inhibited the oxidative stress induced by IAV

The above metabolomics analysis illustrated that NTZ regulated small molecules involved in glutamate metabolism in IAV-infected cells. The important role of glutamic acid metabolism in the antioxidant stress makes us to be interested in the potential of NTZ in resisting the oxidative stress induced by the influenza virus. Therefore, we used DCFH-DA to investigate the ROS changes in PR8 IAV infected cells treated with NTZ. As showed in Figures 7A, B, the production of intracellular ROS was remarkably upregulated 24 h after PR8 IAV infection, which were dose-dependently suppressed by NTZ treatment. Similar suppression were also observed at the different time point of NTZ treatment ($p < 0.001$, Figure 7C).

IAV infection and NTZ treatment associated enzymatic antioxidant activities were measured. As showed in Figure 8, both the activities of CAT and SOD were markedly inhibited by IAV. However, these activities were significantly ameliorated in a dose-dependent manner ($p < 0.05$, Figure 8) after the IAV infected cells were treated with NTZ (3, 6, and 9 $\mu\text{mol/L}$) for 24 h, which confirmed NTZ's antioxidant effects.

NTZ activated the Keap1-Nrf2 pathway

As a key regulator of antioxidant stress, Nrf2 expression and nuclear translocation under NTZ treatment were studied using Western blot analysis. Figure 9A showed that PR8 infection markedly inhibited total expression of total Nrf2 in MDCK cells, and NTZ treatment activated its expression. Furthermore, the expressions of Nrf2 were improved about 15%–25% in nucleus and decreased about 15%–50% in cytoplasm after the IAV infected cells were treated with NTZ at 9 $\mu\text{mol/L}$ (Figure 9B). Meanwhile, Nrf2 treated with 3 and 6 $\mu\text{mol/L}$ of NTZ increased in cytoplasm (Figure 9C) and Keap1 which binds to Nrf2 in the cytoplasm decreased (Figure 9D). To better determine the mechanisms *in vitro*,

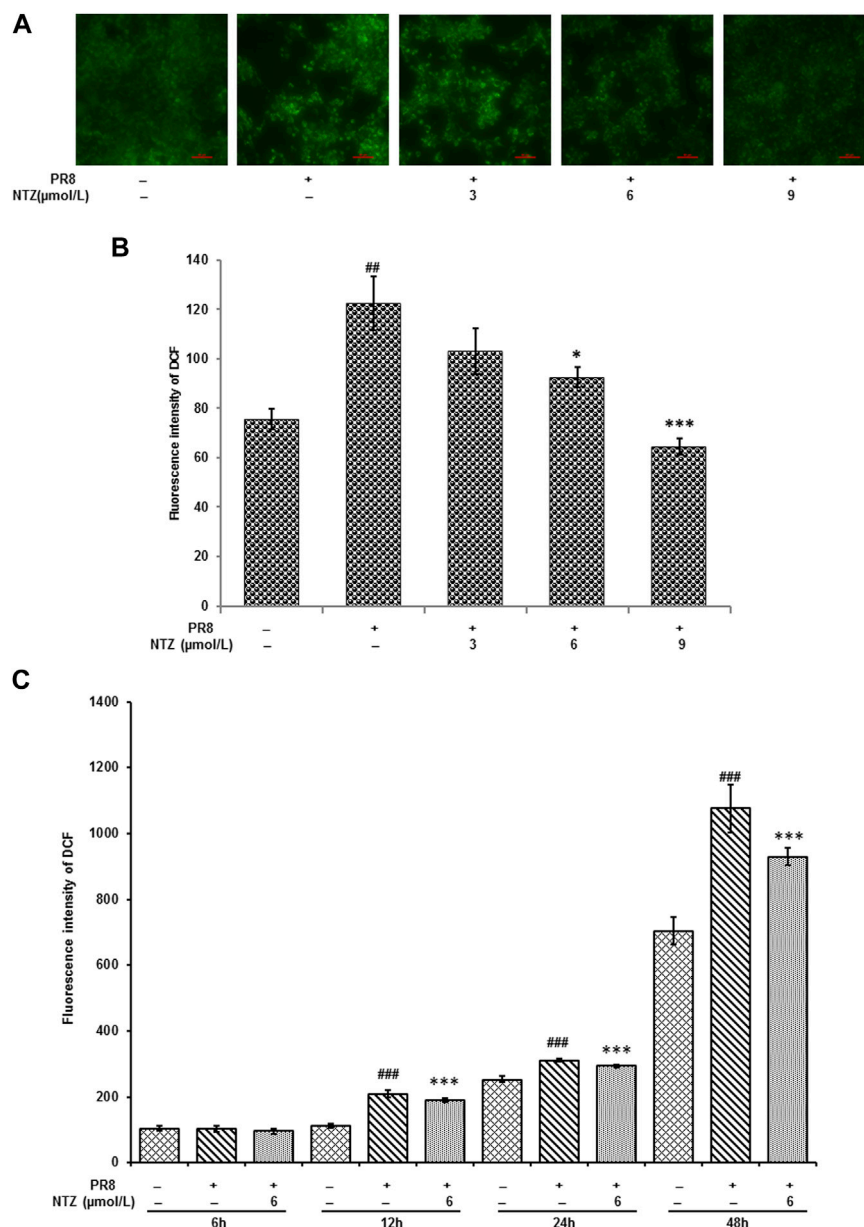
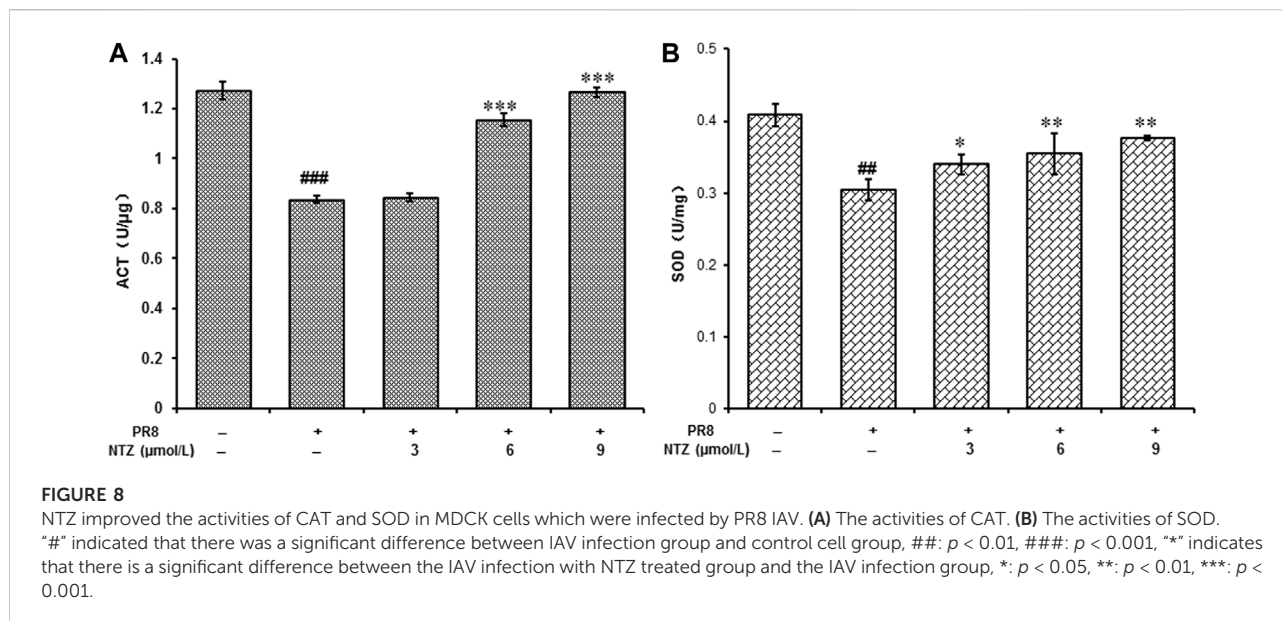


FIGURE 7

NTZ inhibited the productions of intracellular ROS triggered by PR8 IAV infection. **(A)** The fluorescence intensity that intracellular ROS triggered was observed under fluorescence microscope after different treatments for 24 h. **(B)** ROS productions detected by flow cytometer in IAV infected cells were significantly decreased with NTZ increase after treatments for 24 h. **(C)** ROS productions were decreased with different treatment time when IAV infected cells were treated at 6 μmol/L NTZ. “#” indicated that there was a significant difference between IAV infection group and control cell group, ##: $p < 0.01$, ###: $p < 0.001$, “*” indicates that there is a significant difference between the IAV infection with NTZ treated group and the IAV infection group, *: $p < 0.05$, ***: $p < 0.001$.

NQO1, the important downstream molecules in Keap1-Nrf2 pathway, was detected by Western blot analysis. As shown in Figure 9E, after IAV-infected cells being treated with NTZ, the NQO1 level were significantly increased about 5%–30%. The results suggested that NTZ promoted the translocation of Nrf2 to nucleus and activation the downstream genes.

In addition, the expression levels of other proteins, such as PKR, p-eIF2α and LC II, which relate to the biological function of Keap1-Nrf2, were also determined by Western blot analysis. As shown in Figures 9F–H, the expressions of all those three proteins significantly increased in the cells in NTZ treatment groups, compared with those in IAV-infected group. To be



specific, the increased expressions were about 100%–190% (PKR), 5%–40% (p-eIF2 α) and 20%–60% (LC3 II), respectively.

Discussion

Highly pathogenic IAV is still a serious threat to human and animal health in the world. NP of IAV is a highly conserved multifunctional protein that plays an essential role in viral transcription and replication during the virus infection life cycle (Yang et al., 2021). Here, the PR8 IAV proliferation and the expression of NP were suppressed by the thiazolides agent, which documented that NTZ possess a potent anti-influenza A virus activity. More importantly, a LC-MS-based metabolomics approach was used for the first time in this study to identify the changing trend in small molecule metabolites, by which we found the abundance of those metabolites was altered with NTZ treatment in IAV infection MDCK cells, indicating possible novel mechanisms for NTZ against IAV infection. In addition, we revealed a new cellular role for NTZ, which is it could inhibit oxidative stress triggered by PR8 IAV infection through up regulating Nrf2 pathway.

Metabolomics offers novel insights into the network relationship of host, virus and drug, which might contribute toward the understanding of the mechanisms of drug activities (Manchester and Anand, 2017). In this study, we also used UHPLC-QE-MS-based metabolomics to explore the impact of NTZ on MDCK cells during PR8 IAV infection. The metabolomics data presented in metabolic heat maps and OPLS-DA showed that NTZ triggered significant differentiation of small molecule metabolites, deviating from normal and virus-infected samples.

The change of lipid metabolism is a hallmark of IAV infection *in vitro* and *in vivo* (Tanner et al., 2014). In the MDCK cells infected with IAV, the metabolic levels of 2-propylpentanoic acid, 1-hexadecyl-glycero-3-phosphate and other many lipid and lipid-like molecules changed, which proved the regulatory effect of IAV on lipids metabolism. 2-hydroxy-3-methylbutanoic acid and PC [22:5 (7Z, 10Z, 13Z, 16Z, 19Z)/16:1 (9Z)] were the highest increased compounds in NTZ treatment infection cells (group V+N), compared with those in the PR8 IAV infected cells (group V). Both are involved in lipid transport, lipid metabolism and fatty acid metabolism, and play important roles in membrane stability and energy metabolism (Bahado-Singh et al., 2013; Cho et al., 2017). These results suggested that NTZ could regulate the metabolism of lipids and lipid-like molecules following IAV infection. In addition, N-formyl-L-methionine belongs to the class of methionine and derivatives, which leads the initial methionine residue into ribosome as N-formylmethionyl-tRNA, and then initiates the initiation of protein synthesis. The significant increase of N-formyl-L-methionine and (2S)-2-aminopropanoic acid induced by IAV revealed that the virus rapidly synthesized its own protein using MDCK cell elements. The increase of these two metabolites was inhibited by NTZ, implying the inhibitory effect of NTZ on the protein assembly of IAV. Spermidine, L-glutamic acid, and glutamic acid are all small molecules involved in glutamate metabolism, and their changes implied that oxidative stress-related pathways may be involved. By mapping altered expression of all metabolites in group V+N to KEGG, we found that NTZ could regulate the D-glutamine and D-glutamate metabolism, glycerophospholipid metabolism, glycosylphosphatidylinositol (GPI) -anchor biosynthesis and other many metabolic pathways. This suggested that the anti-influenza effect of NTZ may be related to its inhibition of oxidative stress.

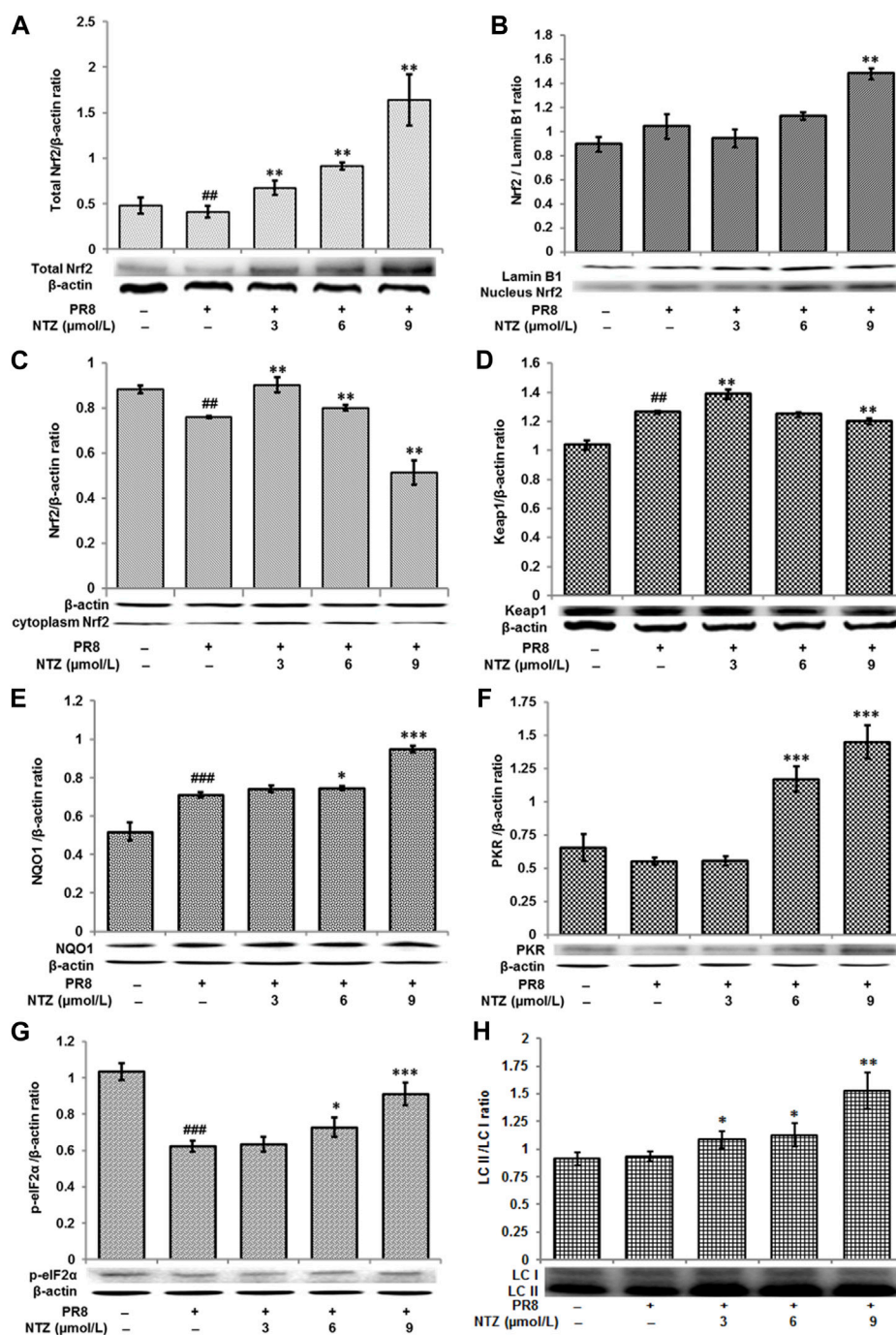


FIGURE 9 Regulation of NTZ on Keap1-Nrf2 pathway. (A–C) The expression levels of Nrf2 in total, nucleus, and cytoplasm in MDCK cells respectively. (D–H) The expression levels of Keap1, NQO1, PKR, p-eIF2α, and LC II in MDCK cells, respectively. “#” indicated that there was a significant difference between IAV infection group and control cell group, #: $p < 0.05$, ##: $p < 0.01$, ###: $p < 0.001$; “*” indicates that there is a significant difference between the IAV infection with NTZ treated group and the IAV infection group, *: $p < 0.05$, **: $p < 0.01$, ***: $p < 0.001$.

The fluctuation in the concentration of eleven metabolites, such as L-glutamic acid, (2S)-5-oxopyrrolidine-2-carboxylic acid and N-formyl-L-methionine, was consistent with the inhibitory

effect of NTZ on IAV replication. L-glutamic acid is one of the 20 proteinogenic amino acids and the main downstream metabolite of glutamine, which plays many important roles in

biological processes (Kou et al., 2021). Meanwhile, L-glutamic acid is related to the synthesis of glutathione, sustaining the redox balance (Yudkoff et al., 1990; Cha et al., 2018). We suspect that the significant increase of L-glutamic acid in group V is associated with the activation of cell's glutathione synthesis and antioxidant effect. It is worth noting that (2S)-5-oxopyrrolidine-2-carboxylic acid is a cyclized derivative of L-glutamic acid and can act as a metabotoxin and acidogen, which is associated with both inborn errors of metabolism and generalized metabolic stress (Yu et al., 2020). The significant IAV-associated increase of (2S)-5-oxopyrrolidine-2-carboxylic acid indicated that L-glutamic acid is not fully been used in the synthesis of glutathione, but also cyclized to form lactam, which thereby reduces the synthesis of glutathione and triggers oxidative stress in cells. Moreover, the significant reduction of 9, 10-epoxyoctadecanoic acid induced by IAV indicated that the virus disturbed the stability of the cell membrane and may cause oxidative stress in the MDCK cells. Fortunately, this mode induced by the virus was suppressed by NTZ, which suggested NTZ could regulate glutathione-related metabolism which played an anti-oxidant and -influenza virus effect.

Influenza virus induces oxidative stress mediated by ROS, which facilitates virus replication (Celestino et al., 2018). Several studies highlighted the importance of redox-sensitive pathways as novel cell-based targets in blocking both viral replication and virus-induced inflammation (Liu et al., 2015; Checconi et al., 2020). In the balance of the intracellular redox state, the Keap-1/Nrf2 pathway plays a critical role (Ramezani et al., 2018). It was demonstrated that Nrf2 is critical for the protective effects on pulmonary inflammation and injury induced by IAV through activating antioxidant genes (Kosmider et al., 2012). The Nrf2-target antioxidant enzymes include SOD, CAT, NQO-1 as well as GST (Tonelli et al., 2018). Tizoxanide is the main metabolite of NTZ, which could remarkably suppress the intracellular ROS induced by lipopolysaccharide in a dose- and time-dependent manner (Shou et al., 2020). NTZ or tizoxanide has been shown to be able to activate PKR and subsequently results in phosphorylation of eIF2- α to block viral replication in HCV and bovine viral diarrhoea virus infected cells (Ashiru et al., 2014; Stachulski et al., 2021). As a marker of autophagy, LC II can be activated by NTZ and further trigger autophagy, which has been reported (Shou et al., 2020). Based on these findings, the upregulation of these proteins may be related to the activation of Nrf2 by NTZ. In this study, we demonstrated that NTZ could inhibit IAV related ROS activation and restore the enzyme activity of CAT and SOD. Furthermore, NTZ may assemble multiple factors to resist IAV infection by promoting the translocation of Nrf2 to the nucleus. Combined with the results of metabolomics analysis, it could be inferred that NTZ inhibits IAV replication by regulating the redox state of cells.

In conclusion, the suppression of IAV replication by NTZ may be due to its interference with the metabolic pathways of

various small molecules that play crucial roles in physiology. The results of NTZ treatment showed that it blocked oxidative stress and facilitated the translocation of Nrf2 to the nucleus, which might play a significant role in the antiviral properties of NTZ against IAV.

Data availability statement

The original contributions presented in the study are included in the article/Supplementary Material, further inquiries can be directed to the corresponding authors.

Author contributions

Conceptualization and Funding acquisition: ZW, KZ; Project administration and Resources: XW, WZ; Roles/Writing—original draft, review & editing: ZW, KZ, ZH, and HZ; Validation: CW, YL; Investigation and Methodology: ZH, YW; Data curation and Formal analysis: KZ, ZH, and HZ. All authors contributed to the article and approved the submitted version.

Funding

This project is supported by the National Natural Science Foundation of China (31872516, 32172913), the National Key Research and Development Program of China (2018YFE0192600).

Acknowledgments

We are very grateful to Dr. Qiaoyang Teng and Zejun Li of SHVRI for they assistance in virus research and Shanghai Biotree biotech Co., Ltd. for the analysis of metabolomics.

Conflict of interest

The authors declare that the research was conducted in the absence of any commercial or financial relationships that could be construed as a potential conflict of interest.

Supplementary material

The Supplementary Material for this article can be found online at: <https://www.frontierspartnerships.org/articles/10.3389/av.2023.11612/full#supplementary-material>

References

- Ashiru, O., Howe, J. D., and Butters, T. D. (2014). Nitazoxanide, an antiviral thiazolide, depletes ATP-sensitive intracellular Ca(2+) stores. *Virology* 462–463, 135–148. doi:10.1016/j.virol.2014.05.015
- Bahado-Singh, R. O., Akolekar, R., Mandal, R., Dong, E., Xia, J., Kruger, M., et al. (2013). Metabolomic analysis for first-trimester Down syndrome prediction. *Am. J. Obstet. Gynecol.* 208, 371 e1–e8. doi:10.1016/j.ajog.2012.12.035
- Bernasconi, D., Amici, C., La Frazia, S., Ianaro, A., and Santoro, M. G. (2005). The IκB kinase is a key factor in triggering influenza A virus-induced inflammatory cytokine production in airway epithelial cells. *J. Biol. Chem.* 280, 24127–24134. doi:10.1074/jbc.m413726200
- Celestino, I., Checconi, P., Amatore, D., De Angelis, M., Coluccio, P., Dattilo, R., et al. (2018). Differential redox state contributes to sex disparities in the response to influenza virus infection in male and female mice. *Front. Immunol.* 9, 1747. doi:10.3389/fimmu.2018.01747
- Cha, Y. J., Kim, E. S., and Koo, J. S. (2018). Amino acid transporters and glutamine metabolism in breast cancer. *Int. J. Mol. Sci.* 19, 907. doi:10.3390/ijms19030907
- Checconi, P., De Angelis, M., Marcocci, M. E., Fraternali, A., Magnani, M., Palamara, A. T., et al. (2020). Redox-modulating agents in the treatment of viral infections. *Int. J. Mol. Sci.* 21, 4084. doi:10.3390/ijms21114084
- Cho, K., Moon, J. S., Kang, J. H., Jang, H. B., Lee, H. J., Park, S. I., et al. (2017). Combined untargeted and targeted metabolomic profiling reveals urinary biomarkers for discriminating obese from normal-weight adolescents. *Pediatr. Obes.* 12, 93–101. doi:10.1111/ijpo.12114
- Dubreuil, L., Houcke, I., Mouton, Y., and Rossignol, J. F. (1996). *In vitro* evaluation of activities of nitazoxanide and tizoxanide against anaerobes and aerobic organisms. *Antimicrob. Agents Chemother.* 40, 2266–2270. doi:10.1128/aac.40.10.2266
- Kosmider, B., Messier, E. M., Janssen, W. J., Nahreini, P., Wang, J., Hartshorn, K. L., et al. (2012). Nrf2 protects human alveolar epithelial cells against injury induced by influenza A virus. *Respir. Res.* 13, 43. doi:10.1186/1465-9921-13-43
- Kou, F., Zhu, B., Zhou, W., Lv, C., Cheng, Y., and Wei, H. (2021). Targeted metabolomics reveals dynamic portrayal of amino acids and derivatives in triple-negative breast cancer cells and culture media. *Mol. Omics* 17, 142–152. doi:10.1039/d0mo00126k
- Lindstrom, S., Garten, R., Balish, A., Shu, B., Emery, S., Berman, L., et al. (2012). Human infections with novel reassortant influenza A(H3N2)v viruses, United States, 2011. *Emerg. Infect. Dis.* 18, 834–837. doi:10.3201/eid1805.111922
- Liu, B., Fang, M., He, Z., Cui, D., Jia, S., Lin, X., et al. (2015). Hepatitis B virus stimulates G6PD expression through HBx-mediated Nrf2 activation. *Cell Death Dis.* 6, e1980. doi:10.1038/cddis.2015.322
- Manchester, M., and Anand, A. (2017). Metabolomics: Strategies to define the role of metabolism in virus infection and pathogenesis. *Adv. Virus Res.* 98, 57–81. doi:10.1016/bs.aivir.2017.02.001
- Odingo, J., Bailey, M. A., Files, M., Early, J. V., Alling, T., Dennison, D., et al. (2017). *In vitro* evaluation of novel nitazoxanide derivatives against *Mycobacterium tuberculosis*. *ACS Omega* 2, 5873–5890. doi:10.1021/acsomega.7b00892
- Ramezani, A., Nahad, M. P., and Faghihloo, E. (2018). The role of Nrf2 transcription factor in viral infection. *J. Cell Biochem.* 119, 6366–6382. doi:10.1002/jcb.26897
- Ritter, J. B., Wahl, A. S., Freund, S., Genzel, Y., and Reichl, U. (2010). Metabolic effects of influenza virus infection in cultured animal cells: Intra- and extracellular metabolite profiling. *BMC Syst. Biol.* 4, 61. doi:10.1186/1752-0509-4-61
- Rossignol, J. F., La Frazia, S., Chiappa, L., Ciucci, A., and Santoro, M. G. (2009). Thiazolides, a new class of anti-influenza molecules targeting viral hemagglutinin at the post-translational level. *J. Biol. Chem.* 284, 29798–29808. doi:10.1074/jbc.m109.029470
- Rossignol, J. F. (2014). Nitazoxanide: A first-in-class broad-spectrum antiviral agent. *Antivir. Res.* 110, 94–103. doi:10.1016/j.antiviral.2014.07.014
- Shou, J., Kong, X., Wang, X., Tang, Y., Wang, C., Wang, M., et al. (2019). Tizoxanide inhibits inflammation in LPS-activated RAW264.7 macrophages via the suppression of NF-κB and MAPK activation. *Inflammation* 42, 1336–1349. doi:10.1007/s10753-019-00994-3
- Shou, J., Wang, M., Cheng, X., Wang, X., Zhang, L., Liu, Y., et al. (2020). Tizoxanide induces autophagy by inhibiting PI3K/Akt/mTOR pathway in RAW264.7 macrophage cells. *Arch. Pharm. Res.* 43, 257–270. doi:10.1007/s12272-019-01202-4
- Stachulski, A. V., Taujanskas, J., Pate, S. L., Rajoli, R. K. R., Aljayyousi, G., Pennington, S. H., et al. (2021). Therapeutic potential of nitazoxanide: An appropriate choice for repurposing versus SARS-CoV-2? *ACS Infect. Dis.* 7, 1317–1331. doi:10.1021/acsinfectdis.0c00478
- Tanner, L. B., Chng, C., Guan, X. L., Lei, Z., Rozen, S. G., and Wenk, M. R. (2014). Lipidomics identifies a requirement for peroxisomal function during influenza virus replication. *J. Lipid Res.* 55, 1357–1365. doi:10.1194/jlr.m049148
- Tian, X., Zhang, K., Min, J., Chen, C., Cao, Y., Ding, C., et al. (2019). Metabolomic analysis of influenza A virus A/WSN/1933 (H1N1) infected A549 cells during first cycle of viral replication. *Viruses* 11, 1007. doi:10.3390/v11111007
- Tonelli, C., Chio, I. I. C., and Tuveson, D. A. (2018). Transcriptional regulation by Nrf2. *Antioxid. Redox Signal* 29, 1727–1745. doi:10.1089/ars.2017.7342
- Wiklund, S., Johansson, E., Sjöström, L., Mellerowicz, E. J., Edlund, U., Shockcor, J. P., et al. (2008). Visualization of GC/TOF-MS-based metabolomics data for identification of biochemically interesting compounds using OPLS class models. *Anal. Chem.* 80, 115–122. doi:10.1021/ac0713510
- Yang, F., Pang, B., Lai, K. K., Cheung, N. N., Dai, J., Zhang, W., et al. (2021). Discovery of a novel specific inhibitor targeting influenza A virus nucleoprotein with pleiotropic inhibitory effects on various steps of the viral life cycle. *J. Virol.* 95, e01432–20. doi:10.1128/jvi.01432-20
- Yu, W., Chen, Y., Putluri, N., Coarfa, C., Robertson, M. J., Putluri, V., et al. (2020). Acquisition of cisplatin resistance shifts head and neck squamous cell carcinoma metabolism toward neutralization of oxidative stress. *Cancers (Basel)* 12, 1670. doi:10.3390/cancers12061670
- Yudkoff, M., Pleasure, D., Cregar, L., Lin, Z. P., Nissim, I., Stern, J., et al. (1990). Glutathione turnover in cultured astrocytes: Studies with [15N]glutamate. *J. Neurochem.* 55, 137–145. doi:10.1111/j.1471-4159.1990.tb08831.x
- Zhang, K., Zheng, W., Zheng, H., Wang, C., Wang, M., Li, T., et al. (2014). Identification of oxidative stress and responsive genes of HepG2 cells exposed to quercetin, and compared with its metabolites. *Cell Biol. Toxicol.* 30, 313–329. doi:10.1007/s10565-014-9287-0
- Zhao, L., Yan, Y., Dai, Q., Li, X., Xu, K., Zou, G., et al. (2020). Development of novel anti-influenza thiazolides with relatively broad-spectrum antiviral potentials. *Antimicrob. Agents Chemother.* 64, e00222–20. doi:10.1128/aac.00222-20